

The HYENAS project: a prediction for the X-ray undetected galaxy groups

Weiguang Cui,^{1,2,3*} Fred Jennings,³ Romeel Dave,^{3,4} Arif Babul^{5,6,7} and Ghassem Gozaliasl^{8,9}

¹ Departamento de Física Teórica, M-8, Universidad Autónoma de Madrid, Cantoblanco 28049, Madrid, Spain

² Centro de Investigación Avanzada en Física Fundamental, (CIAFF), Universidad Autónoma de Madrid, Cantoblanco, 28049 Madrid, Spain

³ Institute for Astronomy, University of Edinburgh, Royal Observatory, Blackford Hill, Edinburgh EH9 3HJ, UK.

⁴ Department of Physics and Astronomy, University of the Western Cape, Robert Sobukwe Rd, Cape Town 7460, South Africa

⁵ Department of Physics and Astronomy, University of Victoria, 3800 Finnerty Road, Victoria, V8P 1A1, BC, Canada

⁶ Infosys Visiting Chair Professor, Indian Institute of Science, Bangalore, 560012, India

⁷ Leverhulme Visiting Professor, Institute for Astronomy, University of Edinburgh, Blackford Hill, Edinburgh, EH9 3HJ, Scotland, UK

⁸ Department of Computer Science, Aalto University, P. O. Box 15400, Espoo, FI-00076, Uusimaa, Finland

⁹ Department of Physics, University of Helsinki, P. O. Box 64, Helsinki, FI-00014, Uusimaa, Finland

Accepted XXX. Received YYY; in original form ZZZ

ABSTRACT

Galaxy groups contain the majority of bound mass with a significant portion of baryons due to the combination of halo mass and abundance (Cui 2024). Hence they serve as a crucial missing piece in the puzzle of galaxy formation and the evolution of large-scale structures in the Universe. In observations, mass-complete group catalogues are normally derived from galaxy redshift surveys detected through various three-dimensional group-finding algorithms. Confirming the reality of such groups, particularly in the X-rays, is critical for ensuring robust studies of galaxy evolution in these environments. Recent works have reported numerous optical groups that are X-ray undetected (see, e.g., Popesso et al. 2024), sparking debates regarding the reasons for the unexpectedly low hot gas fraction in galaxy groups. To address this issue, we utilise zoomed-in simulations of galaxy groups from the novel HYENAS project to explore the range of hot gas fractions within galaxy groups and investigate the intrinsic factors behind the observed variability in X-ray emission. We find that the halo formation time can play a critical role – we see that groups in halos that formed earlier exhibit up to an order of magnitude brighter X-ray luminosities compared to those formed later. This suggests that undetected X-ray groups are preferentially late-formed halos and highlights the connection between gas fraction and halo formation time in galaxy groups. Accounting for these biases in galaxy group identification is essential for advancing our understanding of galaxy formation and achieving precision in cosmological studies.

Key words: keyword1 – keyword2 – keyword3

1 INTRODUCTION

Galaxy groups, typically with a halo mass in the range of $\sim 10^{13} - 10^{14} M_{\odot}$ (Liang et al. 2016), contain the majority of galaxies in the Universe and serve as the primary environment for key galaxy evolution processes such as galaxy transformation driven by the interplay between galaxies and their surrounding gaseous halos (O’Sullivan et al. 2017). Galaxy groups offer valuable insights into fundamental physical processes such as galaxy quenching via active galactic nuclei (AGN) feedback (see, e.g., Bahar et al. 2024; Yang et al. 2024; Eckert et al. 2024), heating and cooling of the intra-group medium (Oppenheimer et al. 2021), the diverse kinematical and morphological properties of their central galaxies (e.g., Loubser et al. 2018; Jung et al. 2022), and the departure from self-similarity observed in clusters (see, e.g., Yang et al. 2022). Furthermore, galaxy groups offer constraints on galaxy formation, cosmological parameters, black hole–galaxy co-evolution, and environmental transformation (see, e.g., Lovisari et al. 2021; Eckert et al. 2021; Oppenheimer et al. 2021, for recent reviews).

Despite their importance, galaxy groups have not received as much attention as galaxy clusters, mainly due to the difficulty in their detection. They are faint in the X-rays, with the temperature of the diffuse gas typically ranging from approximately 0.3 keV to 2 keV (e.g., Mulchaey 2000; Liang et al. 2016), resulting in X-ray luminosities typically ranging from $\sim 10^{40} - 10^{43}$ erg/s which is several orders of magnitude lower than clusters (Lovisari et al. 2021, and references therein). Additionally, they contain far fewer member galaxies than clusters, typically ranging from a few to several dozen (George et al. 2011), which makes them more challenging to identify robustly via group-finding algorithms. This can further lead to false identifications due to chance projections (see, e.g., Pearson et al. 2017; Li et al. 2022). Detecting hot gas in low-mass galaxy groups (i.e., $M_h \in 10^{12.5-13.5} M_{\odot}$) is often regarded as the gold-standard for validation, but their X-ray faintness limits the number of verified low-mass groups and biases them towards lower redshifts ($z < 0.4$) (see, e.g., O’Sullivan et al. 2017; Gozaliasl et al. 2019). Although optical and X-ray surveys continue to improve, it is critical to understand any biases introduced by group selection in order to interpret observations properly.

As an example, the scatter in their properties can introduce Malmquist biases in the inferred physical characteristics (Gozaliasl

* E-mail: weiguang.cui@uam.es; Talento-CM fellow

et al. 2020). Damsted et al. (2023) noted a significant increase in the scatter of L_X compared to other mass proxies below a redshift of 0.15, primarily in low-mass clusters, which hampers the effectiveness of X-ray observations in providing a comprehensive understanding of these groups. Recent studies Khalil et al. (2024) corroborated these findings using the AXES-2MRS galaxy groups, which combined data from the ROSAT All-Sky Survey (RASS) with the Two Micron Redshift Survey (2MRS) Bayesian Group Catalogue. They further suggested that both feedback mechanisms and halo concentration are the reasons for the substantial scatter in the properties of X-ray groups, emphasising that the scatter of scaling relations offers valuable insights into the underlying physics of galaxy groups.

The large variations in the X-ray brightness among galaxy groups can result in legitimately significant groups remaining undetected in X-ray surveys. It has been proposed that only galaxy groups with a central elliptical galaxy tend to exhibit diffused X-ray emission (e.g., Mulchaey et al. 2003, and references therein), a phenomenon contingent upon the detection limits of X-ray telescopes. Utilising the Chandra X-ray Observatory, Pearson et al. (2017) investigated 10 relaxed galaxy groups carefully selected from the GAMA optical galaxy catalogue to mitigate spurious and projection effects. They observed that nine out of ten groups were underluminous in X-rays by a mean factor of approximately 4 compared to typical X-ray-selected samples. Hence, the converse practice of identifying X-ray samples and then seeking their counterparts in optically selected group catalogues may also introduce biases. Recent work by Damsted et al. (2024) expanded the findings of Manolopoulou et al. (2021) from galaxy clusters to galaxy groups – galaxy clusters/groups in overdense environments tend to have higher X-ray luminosities, which they hypothesised is driven by halo assembly bias. Another recent work by Popesso et al. (2024) directly combined data from eROSITA with the updated GAMA catalogue, revealing that 157 out of 189 systems with $M_{200} \geq 10^{13} M_\odot$ and $z < 0.2$ remained undetected in X-rays. Hence, there are significant biases introduced either when selecting groups in the optical or the X-ray (see recent findings, e.g., O’Sullivan et al. 2017; Popesso et al. 2024). Quantifying these biases and understanding their physical origin is essential for groups to be leveraged for galaxy formation and cosmological studies.

In this work, we examine the physical origin of the scatter in properties of galaxy groups using the HYENAS suite of group-scale zoom simulations (see §2 for details). HYENAS is a new suite that re-simulates 120 group-size halos drawn from a large-volume cosmological simulation employing the successful SIMBA galaxy formation model (Davé et al. 2019). Its novelty lies in its selection, which is based on bins in both halo mass and halo formation time. The latter is often implicated as a key driver in the scatter in galaxy group properties (see, e.g. Cui et al. 2021). Here we investigate what implications the variations in group halo formation times can have on their detectability in X-ray and optical surveys, and thereby quantify associated selection biases.

2 THE HYENAS PROJECT

The HYENAS project is a branch of the SIMBA with its focus on galaxy groups using the zoom re-simulation technique. While there have been many cluster-scale zoom projects, for example, the 300 project (Cui et al. 2018), group-scale zooms are less common. One reason is that large-volume cosmological simulations already contain many groups. However, when selected carefully, zooms can sample outliers in the distribution that are not well represented in a random sample. Also, zooms offer the opportunity to achieve higher resolution at a

Table 1. The cosmology parameters used in the SIMBASimulations.

H0 [$km/s/Mpc$]	Ω_Λ	Ω_m	Ω_b	σ_8	n_s
68	0.7	0.3	0.048	0.82	0.97

modest computational cost, enabling resolution convergence studies, though, in this introductory work, we do not employ that aspect of HYENAS.

Besides selecting zoom halos in the group mass regime, HYENAS further selects objects with a wide range in halo formation times. This is motivated by Cui et al. (2021) who argued that halo formation time is the key determinant of the scatter in the stellar-to-halo mass relation, as well as the cold vs. hot gas content of halos. This will presumably also impact the X-ray properties of these systems, which is relevant for this work. Next, we describe the sample selection and X-ray analysis of the HYENAS zoom suite.

2.1 The HYENAS sample and IC generation

The simulation code and parameter choices used are identical to that in the SIMBA simulation, described in Davé et al. (2019) and many subsequent papers. For brevity, we do not repeat these here but focus on the aspects novel to the HYENAS zoom suite.

To increase the sample of galaxy groups, we first run a $200 h^{-1} Mpc$ dark-matter-only simulation ($8 \times$ SIMBA’s volume), with the same dark matter particle mass resolution and *Planck*-concordant cosmology (see Table 1) as SIMBA using Gadget-4 (Springel et al. 2021). From this we select 120 (out of $\sim 10k$) halos with $M_{200c} \in 10^{12.5} - 10^{14} M_\odot$ (where ‘200c’ denotes 200 times the critical density). However, these are not selected randomly; rather, within each 0.5-dex mass bin, we select the galaxies covering a spread halo formation times in percentile bins. The formation time is calculated as the time when half the $z = 0$ halo mass has assembled within the halo’s main progenitor. Gadget-4’s on-the-fly merger tree generation makes this calculation straightforward.

Figure 1 shows the sample selected in 5 halo mass bins and 8 formation time bins, with the latter chosen with percentile bounds of 0-2-5-20-50-80-95-98-100 within each mass bin, and are marked as green dotted horizontal lines in Figure 1. Inside each region in this space, we randomly select three halos to re-simulate. The central galaxy’s density map of one example within each region is shown as an inset image. Note that this is only for illustration, as the image covers 4 times the galaxy’s half-mass radii by blending both stars and dark matter with arbitrary normalisation using the Py-SPHViewer.

The large N-body volume’s random initial conditions are generated using MUSIC (Hahn & Abel 2011), which conveniently allows us to generate these zoomed-in ICs for the HYENAS sample using the same underlying white noise file. For each selected halo, we track all these dark matter particles within the halo at $z = 0$ to their initial condition positions. To precisely identify the centre of the resimulation region in the IC, we also track these particles lying in the centre (minimum potential positions) of the halo ($5 h^{-1} kpc$) and use the mean position of these central particles within the IC as the ‘ref_center’ parameter for MUSIC. Then, we calculate the distances from the IC central position to all the halo particle positions. The 2 times maximum distance rescaled to the simulation boxsize is used for the ‘ref_extent’ parameter for MUSIC to make sure the interested central halo is out of contamination.

Each zoomed-in halo has its ICs generated with three different levels of resolution: Level 0 cuts out the zoomed-in region in the

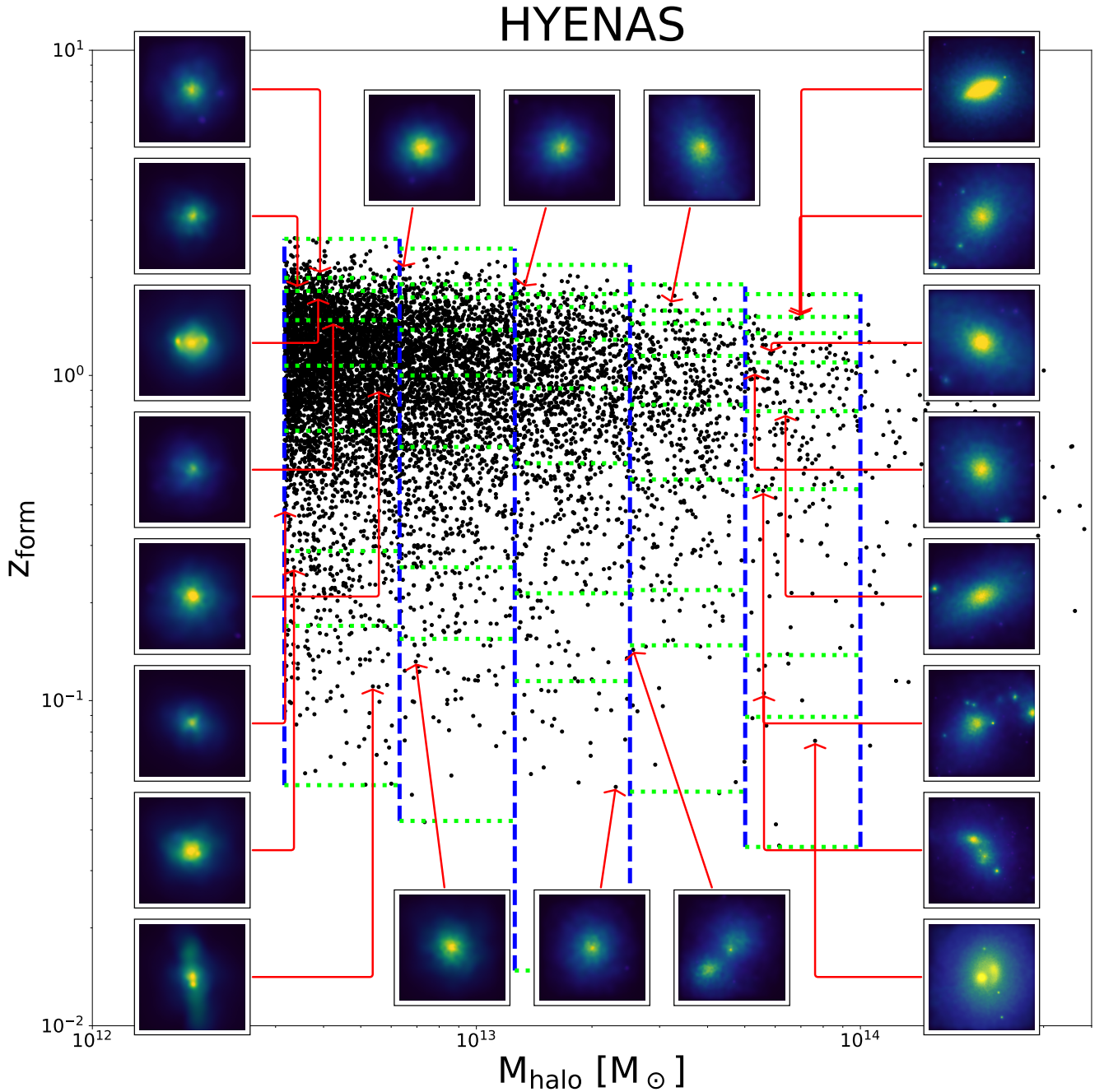


Figure 1. The halo mass – formation time relation from the parent dark-matter-only simulation with illustrations of the selected HYENAS sample. The vertical blue dashed lines mark the 5 halo mass bins, while the horizontal green dotted lines indicate the z_{form} percentile bins. The inset images are the blended gas and star distributions around the central galaxy of the selected HYENAS samples using the Py-SPHViewer package.

IC, adds gas particles, and decreases the resolution outside of the zoomed-in region, which is controlled by the MUSIC code. This results in a dark matter particle mass of $6.513 \times 10^7 h^{-1} M_{\odot}$ and gas element mass of $1.241 \times 10^7 h^{-1} M_{\odot}$, and a minimum gravitational softening of $0.5 h^{-1} \text{kpc}$. Level 1 increases the zoomed-in region’s resolution by 1 level higher with a new white noise at this resolution level. The white noise is consistent as Level0 for these low-resolution levels decreased outside the zoomed-in region. The Level 1 suite has $8\times$ lower particle masses and $2\times$ lower minimum softening. Level 2 has a resolution that is higher than Level 1, with the outside low-

resolution region being consistent with Level 1. Thus, each of the 120 selected HYENAS halo has 3 ICs with different resolutions. Though all the 120 HYENAS halos have both dark-matter-only and hydro ICs, we only run the hydrodynamic for the 40 selected ‘elite’ halo for Level 1 and Level 2, which is still not fully finished due to their very high computation cost. The ‘elite’ sample is the one out of the three random samples with the smallest number of high-resolution particles.

2.2 The HYENAS catalogue and analysis

We output 151 snapshots for each simulation run from $z = 20$ to $z = 0$. Besides the on-fly FoF catalogue from GIZMO and the CAESAR catalogue based on it, we also run the AHF halo finder (Knollmann & Knebe 2009) to identify the halos within R_{200c} and produce an AHF-Caesar catalogue following Chen et al. (2024).

Although there are other (uncontaminated) halos inside the high-resolution zoomed-in regions, we only focus on these originally selected HYENAS halos in this paper. It is also recommended for all papers using the HYENAS data. As such, we need to identify these selected halos properly. Unfortunately, the particle IDs of these halos chosen from the parent dark-matter-only simulation are scrambled within these zoom ICs generated by MUSIC. Thus, we adopted another method to cross-match these halos based on the particle IDs of these zoom ICs. Since we know the exact halo centre position in these ICs, we use the IDs of dark matter particles within $300 h^{-1} \text{kpc}$ (more-or-less corresponding to the $5 h^{-1} \text{kpc}$ radius of halos central regions at $z = 0$) and track them down to $z = 0$ to get their median positions. This position's distances to the $z = 0$ halo centres are used to select the closest halo. If the halo mass difference from the original N-body one is less than 1.5 times, the halo is matched. If not, we choose the halo within the distance of R_{200c} with the closest mass as the matched halo. Only seldom does this happen for these late-formed halos due to the slight evolution difference between dark matter and hydro runs. After finding the matched halos for both FoF and AHF catalogues, we compared the matched halo masses, which basically agree with previous findings (for example Cui et al. 2012, 2014, minor effects due to the baryons). We further calculate the formation redshifts using both FoF and AHF halo catalogues, which are compared to the original halo formation redshift. There is a slightly larger scatter compared to the halo mass differences, primarily coming from the $z_{form} \lesssim 0.3$ sample.

2.3 X-ray luminosities

X-ray properties are calculated using MOXHA package (Jennings & Davé 2023), which combines the yT-based PyXSIM (Biffi et al. 2012, 2013; ZuHone et al. 2014) and Caesar (Turk et al. 2011) software packages with the XSPEC spectral fitting package to provide an end-to-end pipeline for creating mock X-ray photon maps and analysing them to obtain mock observations such as X-ray luminosities, temperatures, and metallicities. First, we make a cut on the cold gas to remove ISM particles, which are artificially pressurised to resolve the Jeans mass (Davé et al. 2019). We use a cut such that only gas particles with a density $\rho < 0.1 m_p \text{ cm}^{-3}$ and temperature $T > 2 \times 10^5 \text{ K}$ are included. Furthermore, we remove all wind particles and all particles with a non-zero star formation rate. We then use PyXSIM to generate X-ray emission fields in the source band of $0.5 - 2.0 \text{ keV}$, using a CIE APEC model (Smith et al. 2001) and using the SIMBA-tracked particle mass fractions for *He, C, N, O, Ne, Mg, Si, S, Ca, Fe* scaled to the Anders & Grevesse (1989) solar abundances table. The other elements are fixed at their solar abundance ratios. We finally sum the luminosity of the hot gas particles within a radius of R_{500} to give our value of $L_{X,0.5-2.0}$. For more details, we refer to Jennings et al. 2024 in prep.

3 RESULTS

3.1 Hot gas fraction

Since the X-ray is coming from hot gas, we first investigate the hot gas mass fraction in both the galaxy groups from both HYENAS (large stars) and SIMBA (small points) simulations and compare them to recent observations from Sun et al. (2009); Laganá et al. (2013); Akino et al. (2022) in Figure 2. First, in agreement with observation, there is a decreasing trend for the $f_{hot \text{ gas}}$ with decreased halo mass. The simulations agree better to the observation data points from Sun et al. (2009); Laganá et al. (2013) (as well as Liang et al. 2016) than those of Akino et al. (2022) at $M_{500} \gtrsim 10^{13.5} M_\odot$. Note that the gas fraction in the massive halo seems to agree better with Akino et al. (2022) as shown in Cui et al. (2018), which could be due to the different AGN feedback strengths. While in the intermediate halo mass range, the simulation data tends to agree with Akino et al. (2022) instead of others (see also Robson & Davé 2020). The disagreements between these observations' results at the galaxy group scale have been discussed in Eckert et al. (2021). Here we would like to add an additional potential cause: Akino et al. (2022) and Eckert et al. (2016) (which also has a lower gas fraction compared to the others) are both based on the XXL survey (Pierre et al. 2016), which is a volume complete survey, while the others mostly preferentially selected the X-ray bright objects. At lower halo mass with $M_{500} \lesssim 10^{13}$, this trend flattens.

Secondly, there is a large scatter of the data points in Figure 2. It is worth noting that the HYENAS sample generally covers the distribution of SIMBA data points well at $M_{500} \gtrsim 10^{13} M_\odot$. These outliers from SIMBA with $f_{hot \text{ gas}} \gtrsim 0.04$ at $M_{500} \lesssim 10^{13} M_\odot$ could be due to the fact that they are close to a massive cluster, as discussed in Cui et al. (2022); in contrast, HYENAS groups are selected to be isolated halos by design. Nevertheless, the agreement of overall distributions between SIMBA and HYENAS suggests that our HYENAS selection criteria are unbiased with respect to halo gas fractions.

The colours of HYENAS points indicate the halo formation redshift as shown by the colourbar in Figure 2. This shows an interesting trend – the gas fraction at a given halo mass correlates with its halo formation time. Late-formed halos tend to have a smaller gas fraction. To statistically show this trend, we separate the data points into $z_{form} > 1$ (red lines) and $z_{form} \leq 1$ (cyan lines). There is quite good agreement between the thick (HYENAS) and thin (SIMBA) lines, and both have a clear separation between early-formed and late-formed halos.

The halo formation time dependence, we speculate, owes to accumulated heating processes from both AGN feedback and shock heating from structure formation. For early-formed halos, it will not only have an early accretion of more cold gas at very high redshift (Cui et al. 2021), experience shock heating earlier and longer but also form its central galaxy earlier with a massive black hole according to the $M_* - M$ relation, which leads to an earlier jet mode feedback in the SIMBA model.

At lower halo mass $M_{500} \lesssim 10^{13} M_\odot$, the late-formed halos tend to have a higher gas fraction than early-formed halos, i.e., a reversed trend, albeit a large error bar for the SIMBA simulation. In comparison, the cross point is at a relatively lower halo mass, $M_{500} \approx 10^{12.5} M_\odot$, for HYENAS, which could be due to the limited number of objects. At this lower halo mass, the jet mode AGN feedback will not turn on because the BH mass (see Cui et al. 2022, for the halo mass – BH mass relation) is lower than the threshold set in SIMBA which is around $10^8 M_\odot$. Thus, the heating process should be dominated by the supernovae feedback, which can be more dominant in these

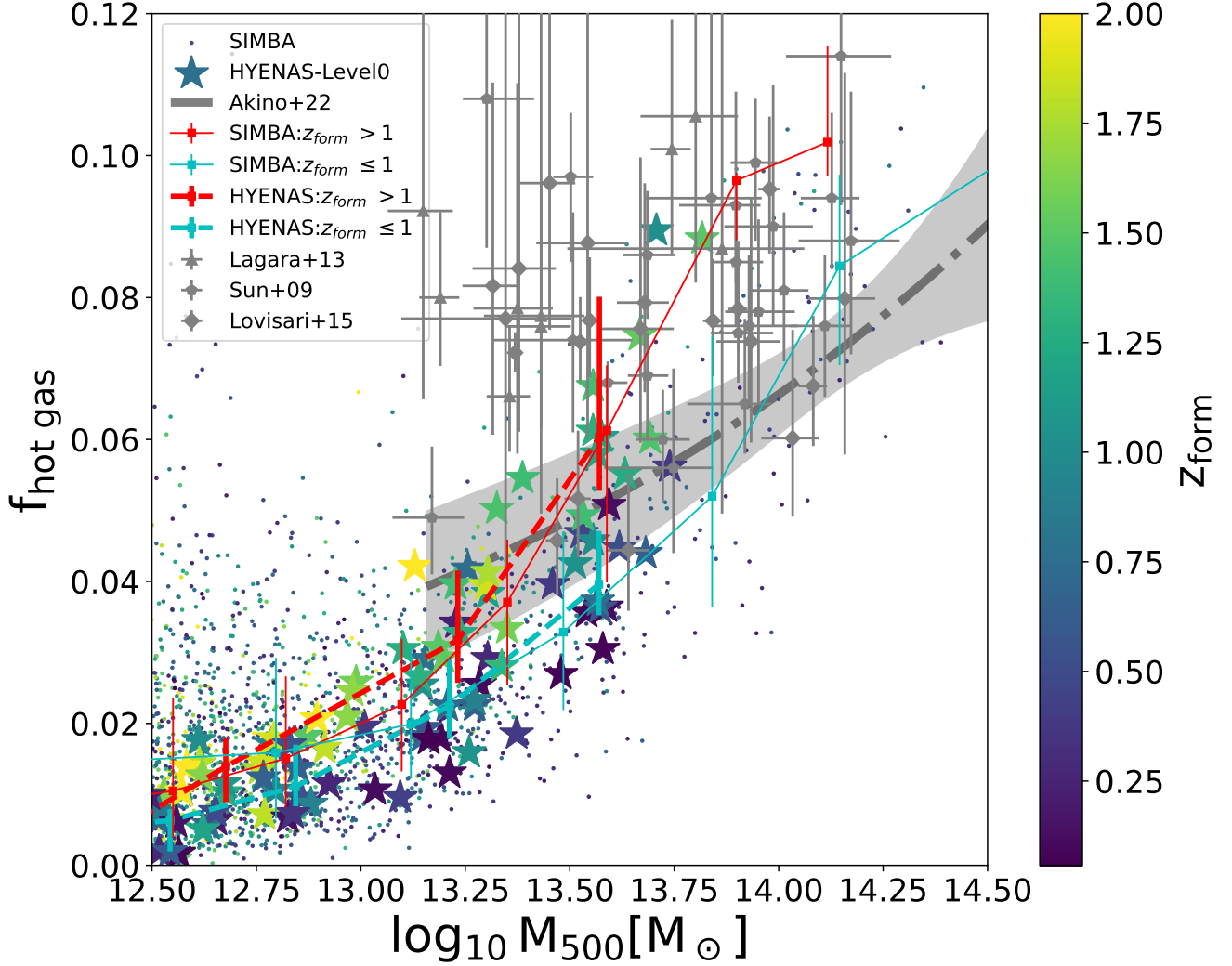


Figure 2. The hot gas fraction as a function of halo mass with colours coding to the halo formation time. The SIMBA simulation results are shown as small dots with the median values in solid thin red and cyan lines for early-formed ($z_{form} > 1$) and late-formed groups ($z_{form} \leq 1$), respectively. The error bars present the 16th – 84th percentile. While the HYENAS sample at Level0 is indicated by stars with the medians in thick dashed lines. The observational results from Sun et al. 2009; Laganá et al. 2013; Lovisari et al. 2015; Akino et al. 2022 are shown in grey symbols with error bars and a dotted-dashed line with a shadow region as indicated in the legend.

late-formed halos with higher star formation. We will return to these explanations in the discussion part in detail.

3.2 X-ray luminosities

In Figure 3, we show the HYENAS groups’ X-ray luminosity within the soft band, [0.5, 2] keV, which has been adopted by many surveys for detecting X-ray galaxy groups. Similar to the hot gas fraction shown in the previous section, the late-formed halos have a lower X-ray luminosity than early-formed ones. The differences between the two families at the same halo mass can be an order of magnitude. Separating the sample by their z_{form} with the arbitrarily selected threshold of $z = 1$, we observe the same trend as shown in Figure 2 with slightly larger separation at $M_{500} \approx 10^{13}$, then a reversed trend at lower halo mass $M_{500} \approx 10^{12.5} M_{\odot}$. As indicated by Bulbul et al. (2024), the detection limit of eRosita at $z \approx 0.2$ (the upper redshift limit in (Popesso et al. 2024)) is around 5×10^{42} ergs/s, which is

indicated by the top horizontal dotted line in Figure 3. If we naively use that as the detection limit of eROSITA at $z = 0.1$, it is clear that some of our simulated halos, even with $M_{500} \sim 5 \times 10^{13} M_{\odot}$ can not be seen.

In comparison, we include the observation results from Anderson et al. (2015), which are based on stacking X-ray emission from the ROSAT All-Sky Survey around the local brightest galaxies. The halo mass in Anderson et al. (2015) is computed using the simulated catalogue of these local brightest galaxies. It is clear that the magenta line is lying in between the HYENAS samples at $M_{500} \geq 10^{13.2} M_{\odot}$, roughly crossing the detection limit, and consistently lying on the top boundary of the HYENAS low mass sample. Similarly, Zhang et al. (2024) stack the X-ray luminosities of the CENhalo sample, which is binned in halo mass M_{200m} based on the group finder algorithm (Tinker 2021). We used the corresponding M_{500c} in Figure 3, which is derived considering the concentration model from Ishiyama et al. (2021). Note that the uncertainty on L_X is estimated from the quadratic sum of the Poisson error, which is not the same as what we

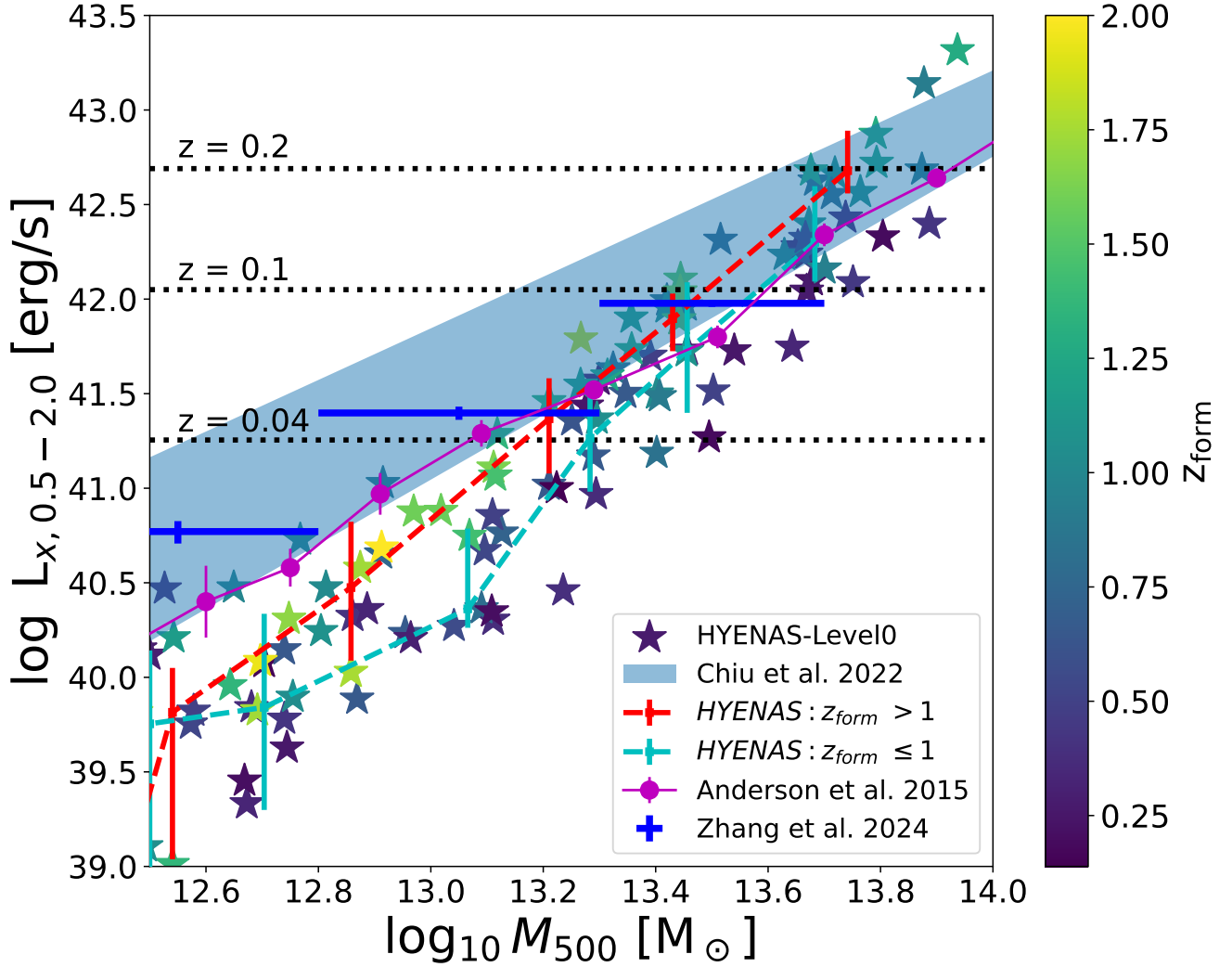


Figure 3. Similar to Figure 2, but for the groups X-ray luminosity. Magenta lines and symbols show the result from Anderson et al. 2015 with the X-ray luminosity estimated at the same energy band – 0.5 - 2.0 keV. Blue error bars are the results from Zhang et al. 2024 using the latest eROSITA survey catalogue. We remind here again that the errorbars are different in simulation (16^{th} – 84^{th} percentiles) from observations.

are showing in HYENAS. Instead of stacking the galaxy groups, Chiu et al. (2022) removed these contaminated systems due to a random superposition. With these remaining 434 groups and clusters, which are cross-confirmed via their weak lensing masses from the HSC survey, they did an MCMC fitting and yielded a similar result to Zhang et al. (2024) as shown in Figure 3. In conclusion, these observation results in the galaxy group scale basically lie on the upper end of the HYENAS result, which could be explained if the observations are missing these X-ray faint groups.

Based on HYENAS data in Figure 3, we further list the roughly predicted limits for eROSITA in Table 2. At each of the three redshifts, we first select all HYENAS halos within ± 10 per cent of the X-ray detection limit. The minimum and maximum halo masses within that L_x limit are listed in the second and third columns of Table 2, respectively. Using the mean (column 4) of columns 2 and 3, we select all halos within a halo mass bin of ± 0.1 , then give the detection fraction in the fifth column of Table 2 as $N_{L_x > L_{x, lim}} / N_{total \text{ in bin}}$. We note here that the HYENAS sample is not a mass-complete one. Therefore, these limits and fractions only serve as a rough prediction. The clear

Table 2. Predicted X-ray detection limits and fractions

redshift	min mass ¹	max mass ²	mean mass ³	fraction ⁴
z	log M_{500}	log M_{500}	log M_{500}	100%
0.2	13.676	13.874	13.775	15.4
0.1	13.444	13.751	13.597	71.4
0.04	13.118	13.495	13.307	70.0

¹ The minimum halo mass in M_\odot above the X-ray luminosity limit at a given redshift, corresponds to 0 per cent detection if the halo mass is smaller than this one.

² The maximum halo mass above the X-ray luminosity limit at a given redshift, corresponds to 100 per cent detection if the halo mass is larger than this one.

³ The mean of columns 2 and 3 for calculating the detection fraction in column 4.

⁴ The fraction of X-ray detected groups within the halo mass bin, column 3 ± 0.1 .

drop of the fraction at $z = 0.2$ presents a good agreement to Popesso et al. (2024). However, we will need a larger sample to confirm this.

4 DISCUSSION AND CONCLUSION

As we have presented before, it is clear that the X-ray-detected galaxy groups are biased toward these gas-rich ones, which are closely linked to their early halo formation time. Although it is easy to understand that – early halo formation will bring more cold gas at high redshift as shown in Cui et al. (2021), those gases will be heated up by either shock heating in structure formation or feedback in the process of galaxy formation – it is unclear how this fits into the picture of general expectations from galaxy formation. We further break this down into three aspects:

- **[Connection to the central galaxy]** Observations have suggested that early-type elliptical galaxies in galaxy groups tend to be associated with diffuse X-ray emission, while late-type disk galaxies do not (Mulchaey et al. 2003). This is especially interesting because Cui et al. (2021) studied the connection between the central galaxy stellar mass and the halo mass and revealed the scatter in that relation is intrinsically driven by halo formation time. In their Supplementary Figure 2, it is clear that early-formed halos tend to host massive quenched galaxies at the same halo mass when $M_{halo} > 10^{13} M_{\odot}$, reversed from the low mass halos in which the red/quenched galaxies with lower stellar mass tend to live in late-formed halos. This is further confirmed by the galaxy age (see Figure D1) if we note that the early-type galaxies are older. We understand that this issue is still in debate; see Scholz-Díaz et al. (2024) for the most recent discussions on that. We argue here that our results (including Cui et al. (2021)) are consistent with their claim that higher stellar mass galaxies at a given halo mass have characteristics of old, red, and passive systems at halo mass larger than $10^{13} M_{\odot}$. While there is less data in Scholz-Díaz et al. (2024) at low halo/stellar mass range to make a solid conclusion, and their total mass is only calculated within $3R_e$.

Due to being driven by halo formation time in both relations, we expect a positive connection between the gas fraction and central galaxy stellar mass at group halo mass scales – more massive galaxies tend to be surrounded by more hot gas. This is proved in Figure B1. As suggested by Correa & Schaye (2020), disc galaxies are less massive than elliptical galaxies in same-mass haloes when the halo mass is larger than $10^{13} M_{\odot}$, which confirms the previous suggestion that elliptical galaxies tend to associate with X-ray emissions.

We further find a positive correlation between the central galaxy mass-weighted age and halo formation time, as shown in Figure D1. This again confirms our results at $M_{500} \gtrsim 10^{13} M_{\odot}$ are consistent with Scholz-Díaz et al. (2024) and lead to a positive correlation with the scatter in central galaxy stellar mass. This is contrary to the findings of Kulier et al. (2019), which could be because they used all galaxies within the EAGLE simulation, so low-mass halos dominate the sample. At low halo masses $M_{halo} \lesssim 10^{13} M_{\odot}$, such an anti-correlation is also found in Cui et al. (2021). We also note that a crossing point is shown in Figure 2, which should be consistent with the reversed trend at low halo mass, though at slightly different halo masses when comparing SIMBA and HYENAS.

- **[The abundance of cold gas]** In previous figures, we only focus on the hot gas mass fraction; it is unclear how the cold gas abundance will contribute to the full picture, i.e. whether the low hot gas fraction is due to a high cold gas fraction or not. This is because galaxy groups, unlike galaxy clusters, tend to host a noticeable fraction of gas mass in cold as well. Investigating that will help us to form a full picture of how they are formed. As expected, the cold gas gradually contributes more to the total gas mass with the halo mass reduced after $M_{500} \lesssim 10^{13.4} M_{\odot}$, see Figure A1. It is further interesting to see that there is more cold gas in late-formed halos than in early-

formed ones in that figure, which we will discuss the reasons for in the following section. That reveals that the history of halo formation also affects the history of gas thermalization.

- **[Connection to central BH]** Although there is more gas in early-formed halos, the gas must be hot to be seen in the X-ray band. Therefore, the heating processes are key to understanding why there is more hot gas in these early-formed halos than in late-formed ones. As shown in the previous section, the early-formed halos not only have more gas but also more hot gas than these late-formed halos (see Figure A1). Thus, early-formed halos should have more heating sources/energies than late-formed ones. One possible reason is shock heating, which should happen earlier in early-formed halos, yielding a hot gas fraction. The other reason is AGN feedback. For example, Liang et al. (2016) suggested that the winds ejected from the group galaxies interact with and heat the hot halo gas, which not only reduces the rate at which the halo gas cools and accumulates in the group’s central galaxies but also causes its distribution to remain more extended. More importantly, we found that the massive galaxies tend to host a more massive BH at the same halo mass (see Davies et al. 2019, 2020, at the more massive halo mass end; see also Ma et al. in prep.). This is not surprising since the early-formed halos tend to form the central galaxy earlier, and as such, the central BH mass grows faster and earlier. For the case of SIMBA model, it enters the jet mode earlier to quench the central galaxy (Cui et al. 2021) with the higher hot gas mass as a by-product. This picture is supported by Figure C1. We are currently working on another paper to record the heating energy from different sources to determine which is more important for gas heating in galaxy groups.

Our findings in this work are based only on the SIMBA baryon model. However, we also investigated the TNG-300 simulation, which shows the same gas fraction trend with a clear separation between early- and late-formed halos, albeit with a little systematically higher values than what is shown in Figure 2 (see also Davies et al. 2020, for the higher gas fraction in TNG than EAGLE). Recent observation work by Popesso et al. (2024), which compared the X-ray detected and undetected groups, also suggested a similar conclusion, i.e., halo assembly bias is the cause. Furthermore, Andreon et al. (2022) showed that under X-ray luminous clusters populate the low concentration of dark matter end of the distribution for a given mass, suggesting that they are late-formed as well. However, the halo formation redshift is very hard to measure in observations. There are ways to approximate it, such as the galaxy magnitude/stellar mass difference in fossil groups (e.g. Jones et al. 2003; Gozaliasl et al. 2014) and the connection between galaxy/gas dynamical state and halo formation time (e.g. Mostoghiu et al. 2019), but all have a substantial uncertainty. Though there are claims that the fossil groups show no difference to normal groups in X-ray scaling relations (e.g. Kundert et al. 2015; Girardi et al. 2014), their lowest X-ray is still above $\sim 10^{42}$, which is much higher compared to the limit shown in this study. In this theoretical investigation, we don’t probe into details but suggest these connections to galaxy and BH properties can be tested in observations as discussed in previous paragraphs.

Another possible explanation for these X-ray faint or undetected galaxy groups is the projection effect when they are generally identified through the galaxy catalogues (see Hernquist et al. 1995, for example). If two small halos are lying along the same line of sight but have a large separation, neither will have large enough hot gas to shine in X-ray, see Figure 3 for how quickly the X-ray luminosity drops with halo mass. However, this projection issue may be solved by highly accurate spectroscopic redshift measurement with proper galaxy velocity distribution modelling.

Lastly, the role that baryonic physics models play in this result is not very clear, especially the AGN feedback, which may affect the X-ray luminosity. For example, [Kar Chowdhury et al. \(2022\)](#) showed that the different versions of SIMBA run turning on and off different SIMBA' models, especially the X-ray AGN feedback and radiative mode, result in different surface brightness profiles at different radii. However, we argue that this will only systematically shift our result, while the effect of halo formation time on the X-ray luminosity will be unchanged, which we have confirmed with the TNG-300 result. On the other hand, many studies with the EAGLE simulation show consistent predictions, as we have discussed before.

ACKNOWLEDGEMENTS

WC is supported by the STFC AGP Grant ST/V000594/1, the Atracción de Talento Contract no. 2020-T1/TIC-19882 was granted by the Comunidad de Madrid in Spain, and the science research grants were from the China Manned Space Project. He also thanks the Ministerio de Ciencia e Innovación (Spain) for financial support under Project grant PID2021-122603NB-C21 and HORIZON EUROPE Marie Skłodowska-Curie Actions for supporting the LACEGAL-III project with grant number 101086388.

FJ would like to acknowledge the support of the Science and Technology Facilities Council (STFC).

AB acknowledges support from the Natural Sciences and Engineering Research Council of Canada (NSERC) through its Discovery Grant program, the Infosys Foundation, via an endowed Infosys Visiting Chair Professorship at the Indian Institute of Science and the Leverhulme Trust.

These HYENAS simulations were performed using the DiRAC@Durham facility managed by the Institute for Computational Cosmology on behalf of the STFC DiRAC HPC Facility (www.dirac.ac.uk) with the DiRAC Project: ACSP252, titled Simba Zoom Simulations of Galaxy Groups. The equipment was funded by BEIS capital funding via STFC capital grants ST/P002293/1, ST/R002371/1 and ST/S002502/1, Durham University, and STFC operations grant ST/R000832/1. DiRAC is part of the National e-Infrastructure. The analysis reported in this paper was also partly enabled by WestGrid and the Digital Research Alliance of Canada (alliancecan.ca).

DATA AVAILABILITY

The data output of this paper is available on GitHub: The HYENAS simulation is currently available upon request, but it will become publicly available very soon.

REFERENCES

- Akino D., et al., 2022, *PASJ*, **74**, 175
- Anders E., Grevesse N., 1989, *Geochimica Cosmochimica Acta*, **53**, 197
- Anderson M. E., Gaspari M., White S. D. M., Wang W., Dai X., 2015, *MNRAS*, **449**, 3806
- Andreon S., Trinchieri G., Moretti A., 2022, *Monthly Notices of the Royal Astronomical Society*, **511**, 4991
- Bahar Y. E., et al., 2024, *arXiv e-prints*, p. [arXiv:2401.17276](https://arxiv.org/abs/2401.17276)
- Biffi V., Dolag K., Böhringer H., Lemson G., 2012, *MNRAS*, **420**, 3545
- Biffi V., Dolag K., Böhringer H., 2013, *MNRAS*, **428**, 1395
- Bulbul E., et al., 2024, *arXiv e-prints*, p. [arXiv:2402.08452](https://arxiv.org/abs/2402.08452)
- Chen M., Cui W., Fang W., Wen Z., 2024, *ApJ*, **966**, 227
- Chiu I. N., et al., 2022, *A&A*, **661**, A11
- Correa C. A., Schaye J., 2020, *Monthly Notices of the Royal Astronomical Society*, **499**, 3578
- Cui W., 2024, *arXiv e-prints*, p. [arXiv:2406.03829](https://arxiv.org/abs/2406.03829)
- Cui W., Borgani S., Dolag K., Murante G., Tornatore L., 2012, *MNRAS*, **423**, 2279
- Cui W., Borgani S., Murante G., 2014, *MNRAS*, **441**, 1769
- Cui W., et al., 2018, *MNRAS*, **480**, 2898
- Cui W., Davé R., Peacock J. A., Anglés-Alcázar D., Yang X., 2021, *Nature Astronomy*, **5**, 1069
- Cui W., et al., 2022, *MNRAS*, **514**, 977
- Damsted S., et al., 2023, *A&A*, **676**, A127
- Damsted S., et al., 2024, *arXiv e-prints*, p. [arXiv:2403.17055](https://arxiv.org/abs/2403.17055)
- Davé R., Anglés-Alcázar D., Narayanan D., Li Q., Rafieferantsoa M. H., Appleby S., 2019, *MNRAS*, **486**, 2827
- Davies J. J., Crain R. A., McCarthy I. G., Oppenheimer B. D., Schaye J., Schaller M., McAlpine S., 2019, *MNRAS*, **485**, 3783
- Davies J. J., Crain R. A., Oppenheimer B. D., Schaye J., 2020, *Monthly Notices of the Royal Astronomical Society*, **491**, 4462
- Eckert D., et al., 2016, *Astronomy and Astrophysics*, **592**, A12
- Eckert D., Gaspari M., Gastaldello F., Brun A. M. C. L., O'Sullivan E., 2021, *Universe*, **7**, 142
- Eckert D., Gastaldello F., O'Sullivan E., Finoguenov A., Brienza M., the X-GAP collaboration 2024, *arXiv e-prints*, p. [arXiv:2403.17145](https://arxiv.org/abs/2403.17145)
- George M. R., et al., 2011, *ApJ*, **742**, 125
- Girardi M., et al., 2014, *Astronomy and Astrophysics*, **565**, A115
- Gozaliasl G., Khosroshahi H. G., Dariush A. A., Finoguenov A., Jassur D. M. Z., Molaiezhad A., 2014, *A&A*, **571**, A49
- Gozaliasl G., et al., 2019, *MNRAS*, **483**, 3545
- Gozaliasl G., et al., 2020, *A&A*, **635**, A36
- Hahn O., Abel T., 2011, *MNRAS*, **415**, 2101
- Hernquist L., Katz N., Weinberg D. H., 1995, *ApJ*, **442**, 57
- Ishiyama T., et al., 2021, *MNRAS*, **506**, 4210
- Jennings F., Davé R., 2023, *MNRAS*, **526**, 1367
- Jones L. R., Ponman T. J., Horton A., Babul A., Ebeling H., Burke D. J., 2003, *Monthly Notices of the Royal Astronomical Society*, **343**, 627
- Jung S. L., et al., 2022, *Monthly Notices of the Royal Astronomical Society*, **515**, 22
- Kar Chowdhury R., Chatterjee S., Paul A., Sarazin C. L., Dai J. L., 2022, *ApJ*, **940**, 47
- Khalil H., Finoguenov A., Tempel E., Mamon G. A., 2024, *arXiv e-prints*, p. [arXiv:2403.17061](https://arxiv.org/abs/2403.17061)
- Knollmann S. R., Knebe A., 2009, *The Astrophysical Journal Supplement Series*, **182**, 608
- Kulier A., Padilla N., Schaye J., Crain R. A., Schaller M., Bower R. G., Theuns T., Paillas E., 2019, *Monthly Notices of the Royal Astronomical Society*, **482**, 3261
- Kundert A., et al., 2015, *Monthly Notices of the Royal Astronomical Society*, **454**, 161
- Laganá T. F., Martinet N., Durret F., Lima Neto G. B., Maughan B., Zhang Y. Y., 2013, *Astronomy and Astrophysics*, **555**, A66
- Li Q., et al., 2022, *ApJ*, **933**, 9
- Liang L., Durier F., Babul A., Davé R., Oppenheimer B. D., Katz N., Fardal M., Quinn T., 2016, *Monthly Notices of the Royal Astronomical Society*, **456**, 4266
- Loubser S. I., Hoekstra H., Babul A., O'Sullivan E., 2018, *Monthly Notices of the Royal Astronomical Society*, **477**, 335
- Lovisari L., Reiprich T. H., Schellenberger G., 2015, *Astronomy and Astrophysics*, **573**, A118
- Lovisari L., Ettori S., Gaspari M., Giles P. A., 2021, *Universe*, **7**, 139
- Manolopoulou M., Hoyle B., Mann R. G., Sahlén M., Nadathur S., 2021, *Monthly Notices of the Royal Astronomical Society*, **500**, 1953
- Mostoghiu R., Knebe A., Cui W., Pearce F. R., Yepes G., Power C., Dave R., Arth A., 2019, *MNRAS*, **483**, 3390
- Mulchaey J. S., 2000, *Annual Review of Astronomy and Astrophysics*, **38**, 289
- Mulchaey J. S., Davis D. S., Mushotzky R. F., Burstein D., 2003, *The Astrophysical Journal Supplement Series*, **145**, 39

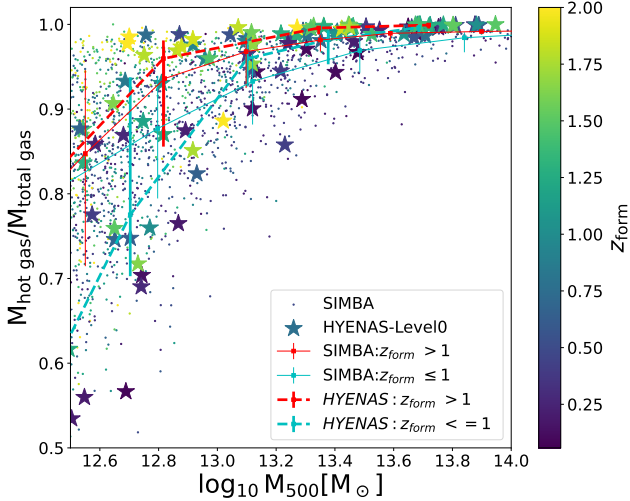


Figure A1. The hot gas mass fraction with respect to the total gas mass. The symbols and lines share the same meanings as Figure 2. The hot gas dominates (≥ 0.95) the total gas mass in halos with $M_{500} \geq 10^{13.4} M_{\odot}$. Cold gas starts to contribute more mass as the halo mass drops. It is also interesting to see that the hot gas fraction is higher in these early-formed halos than in later-formed ones at the same halo mass, which is clearer at the lower halo mass.

- O’Sullivan E., et al., 2017, *Monthly Notices of the Royal Astronomical Society*, 472, 1482
- Oppenheimer B. D., Babul A., Bahé Y., Butsky I. S., McCarthy I. G., 2021, *Universe*, 7, 209
- Pearson R. J., et al., 2017, *MNRAS*, 469, 3489
- Pierre M., et al., 2016, *Astronomy and Astrophysics*, 592, A1
- Popesso P., et al., 2024, *MNRAS*, 527, 895
- Robson D., Davé R., 2020, *MNRAS*, 498, 3061
- Scholz-Díaz L., Martín-Navarro I., Falcón-Barroso J., Lyubenova M., van de Ven G., 2024, *Nature Astronomy*,
- Smith R. K., Brickhouse N. S., Liedahl D. A., Raymond J. C., 2001, *ApJ*, 556, L91
- Springel V., Pakmor R., Zier O., Reinecke M., 2021, *MNRAS*, 506, 2871
- Sun M., Voit G. M., Donahue M., Jones C., Forman W., Vikhlinin A., 2009, *The Astrophysical Journal*, 693, 1142
- Tinker J. L., 2021, *ApJ*, 923, 154
- Turk M. J., Smith B. D., Oishi J. S., Skory S., Skillman S. W., Abel T., Norman M. L., 2011, *The Astrophysical Journal Supplement Series*, 192, 9
- Yang T., Cai Y.-C., Cui W., Davé R., Peacock J. A., Sorini D., 2022, *MNRAS*, 516, 4084
- Yang T., Davé R., Cui W., Cai Y.-C., Peacock J. A., Sorini D., 2024, *MNRAS*, 527, 1612
- Zhang Y., et al., 2024, *arXiv e-prints*, p. arXiv:2401.17309
- ZuHone J. A., Biffi V., Hallman E. J., Randall S. W., Foster A. R., Schmid C., 2014, *arXiv e-prints*, p. arXiv:1407.1783

APPENDIX A: HOT GAS ABUNDANCE

As the halo mass decreases, gas heating becomes weak for various reasons. As such, galaxy groups, unlike clusters, may contain a certain fraction of cold gas, which doesn’t emit X-ray photons. As such, it would be interesting to understand the cold gas content in galaxy groups. In Figure A1, we show the hot gas mass fraction with respect to the total gas mass. Furthermore, the simulation data is coloured and split by their halo formation time. Although hot gas still occupies the most mass in galaxy groups, the decreasing fraction is very clear

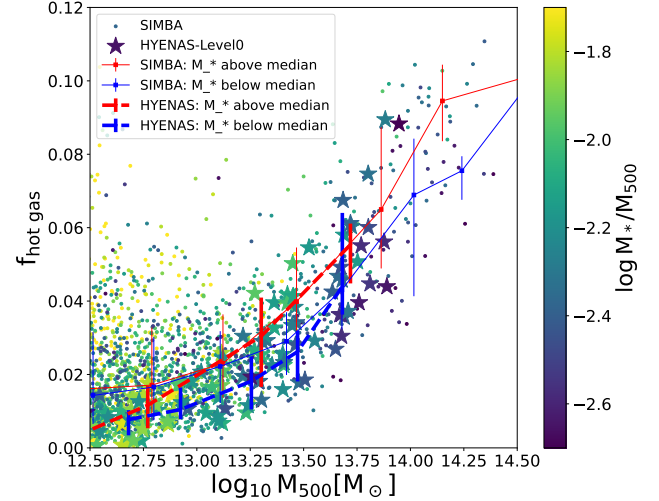


Figure B1. Similar to Figure 2 but color coding to the central galaxy mass fraction. Due to the stellar mass fraction depending on halo mass, we used its median value in the $M_*/M_{halo} - M_{halo}$ to separate the two families. At M_{500} above $10^{13} M_{\odot}$, more massive central galaxies tend to have higher hot gas fractions than less massive galaxies at the same halo mass.

along halo mass, and late-formed halos have systematically more cold gas than early-formed halos.

APPENDIX B: GAS FRACTION SEPARATED BY CENTRAL GALAXY FRACTION

Instead of halo formation time, which directly affects the central galaxy properties (e.g. Cui et al. 2021), we investigate the central galaxy (or brightest group galaxy in observation, BGG) stellar mass fraction’s influence on the hot gas fraction in Figure B1. The symbol colours of simulated objects are with respect to the BGG’s stellar mass fraction $-M_*/M_{500}$. To clearly show its effects, we first estimate the median line in the $M_{500} - M_*/M_{500}$ relation. Then, separate these symbols in Figure B1 into two groups: above the median line or below the median line in the $M_{500} - M_*/M_{500}$ relation. After that, we show the median values of the two groups in red and blue, respectively. The high gas fraction is generally associated with a massive BGG.

APPENDIX C: GAS FRACTION SEPARATED BY CENTRAL BH MASS

Similar to Figure B1, we highlight the effect of black hole mass in Figure C1. It is not surprising to see the halo with a higher black hole mass tends to have more hot gas. This is because we know that the black hole mass is primarily scaling with its host galaxy’s stellar mass. On the other hand, this hints the AGN feedback may play a role in the higher hot gas fraction.

APPENDIX D: GAS FRACTION SEPARATED BY CENTRAL GALAXY AGE

Instead of BGG’s stellar mass fraction, we show the connection to BGG’s mass-weighted stellar age in Figure D1. Again, this fits into the consistent picture of BGGs formed earlier with older age to have more mass in the early-formed halos.

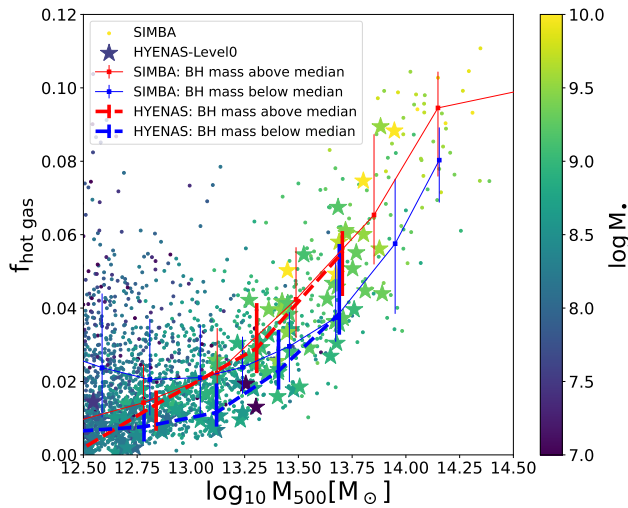


Figure C1. Similar to Figure B1 but colour coding to the BH mass in the central galaxy. Again, we use the median line in the $M_{\bullet} - M_{halo}$ relation to split the massive and low mass BH families. A more massive central BH tends to have a higher gas fraction at the same halo mass range when $M_{500} \gtrsim 10^{13} M_{\odot}$.

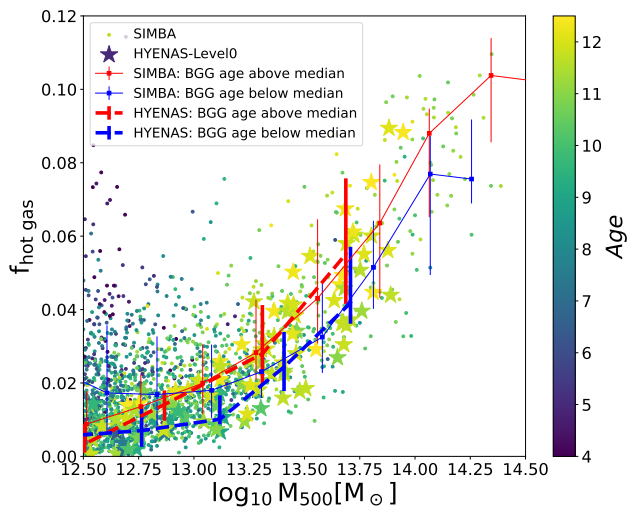


Figure D1. Similar to Figure B1 but colour coding to the stellar age of the central galaxy. Again, we use the median line in the $age - M_{halo}$ relation to split the sample into two galaxy age families. At the same halo mass range with $M_{500} \gtrsim 10^{13} M_{\odot}$, an older galaxy tends to have a higher gas fraction.

This paper has been typeset from a $\text{\TeX}/\text{\LaTeX}$ file prepared by the author.